SAND2013-6539C

Thermally stable imaging channeled spectropolarimetry

Julia Craven-Jones[1], Brandyn M. Way[1], Jeff Hunt[1], Michael W. Kudenov[2], and Jeffrey A. Mercier[1]

[1]Sandia National Laboratories, 1515 Eubank Blvd SE, Albuquerque NM 87123
[2]Department of Electrical and Computer Engineering, North Carolina State University, Raleigh, NC 27695

ABSTRACT

Channeled spectropolarimetry can measure the complete polarization state of light as a function of wavelength. Typically, a channeled spectropolarimeter uses high order retarders made of uniaxial crystal to amplitude modulate the measured spectrum with the spectrally-dependent Stokes polarization information. A primary limitation of conventional channeled spectropolarimeters is related to the thermal variability of the retarders. Thermal variation often forces frequent system recalibration, particularly for field deployed systems. However, implementing thermally stable retarders results in an athermal channeled spectropolarimeter that relieves the need for frequent recalibration. Past work has addressed this issue by developing athermalized retarders using two or more uniaxial crystals. Recently, a retarder made of biaxial KTP and cut at a thermally insensitive angle was used to produce an athermal channeled spectropolarimeter. This paper presents the results of the biaxial crystal system and compares the two thermal stabilization techniques in the context of producing an imaging thermally stable channeled spectropolarimeter. A preliminary design for a snapshot imaging channeled spectropolarimeter is also presented.

1. INTRODUCTION

Channeled spectropolarimetry (CSP) is a no-moving-parts spectropolarimetric measurement technique that can be used with either dispersive or interferometric (Fourier transform) spectrometers [1, 2]. Developed extensively over the past decade, CSP instruments have been demonstrated in the visible and infrared for laboratory-based characterization of materials, remote sensing, and polarimetric imaging (see [3-6] for examples). Typically, a CSP system incorporates two high order uniaxial crystal retarders and an analyzer with a spectrometer, as depicted in Fig. 1. The two retarders, R_1 and R_2, have fast axis orientations of 0^o (along the *y*-axis) and 45^o, respectively, while the analyzer is parallel to R_1 at 0^o. This configuration modulates the measured spectrum with carrier frequencies, the amplitudes of which contain the spectrally-dependent Stokes parameters $S_0(\sigma)$, $S_1(\sigma)$, $S_2(\sigma)$, and $S_3(\sigma)$. The intensity measured by the spectrometer will follow

$$I(\sigma)=\frac{1}{2}\left[S_0(\sigma)+S_1(\sigma)\cos(\phi_2)+S_2(\sigma)\sin(\phi_1)\sin(\phi_2)+S_3(\sigma)\cos(\phi_1)\sin(\phi_2)\right]. \quad (1)$$

In Eq. 1, $\phi_i(\sigma)=2\pi\sigma Bl_i$ is the phase difference introduced by the i^{th} retarder, $B=n_e-n_o$ is the birefringence of the crystal, l_i is the retarder thickness, and $\sigma=1/\lambda$. Thus, with minimal additional complexity, a CSP system provides a complete Stokes polarization measurement that is acquired simultaneously with the spectrometer's spectral measurement.

One technique that is used to polarimetrically calibrate a CSP involves acquiring a reference measurement while observing a target with a known polarization state [7]. The reference data is used to obtain the

phase information associated with the modulating carrier frequencies (ϕ_1 and ϕ_2) produced by the CSP retarder elements. By characterizing the phase terms, the polarization data products can be separated in the modulated spectral measurements.

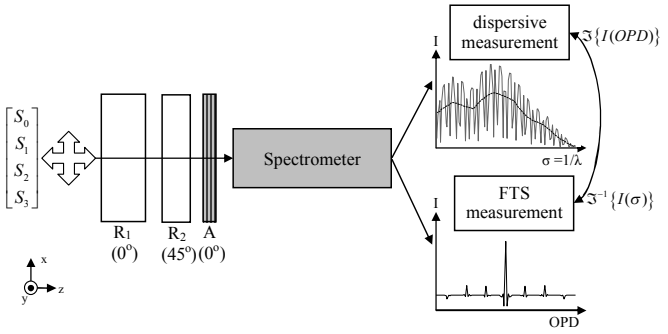

Fig. 1. Schematic of a CSP system. To incorporate a complete polarization measurement, two retarders, R_1 and R_2, and an analyzer A are placed in series before a dispersive of interferometric (FTS) spectrometer.

The primary complication related to this reference beam calibration technique arises when sample data is acquired at a different temperature than the reference. Temperature produces a variation in thickness and dispersion of the birefringent retarder elements, changing in the carrier frequencies in the modulated spectral measurements. The change in phase of the i^{th} retarder for a change of temperature ΔT is given by

$$\Delta\phi_i \approx 2\pi\sigma l_i \Delta T\left[B(\sigma)\gamma_L + \left(\frac{\partial n_e}{\partial T} - \frac{\partial n_o}{\partial T}\right)\right], \tag{2}$$

where $\gamma_L = (1/l_i)(\partial l_i / \partial T)$ is the coefficient of linear thermal expansion along the propagation direction.

Eq. 2 implies that when the calibration data is applied after the instrument experiences a change in temperature, the carrier frequency phases are not effectively removed. This produces calibration errors in the polarization data products. As an example, a visible-near infrared (VNIR) CSP system was simulated assuming 32.5 and 10.8 mm thick quartz retarders that introduce approximately 300 and 100 μm of optical path difference (OPD) for R_1 and R_2, respectively. The simulation used a spectrally invariant incident Stokes vector of $S_{in}/S_0 = [S_0\ S_1\ S_2\ S_3]^T = [1;\ 0.8;\ -0.5;\ 0.3]$. Fig. 2 (a) depicts the calibration error induced by a 5° C change in temperature of the quartz retarders between the acquisition of the reference and sample data. The reconstructed and known Stokes values are plotted to illustrate the significant deviation of the reconstructed values versus the true input polarization state.

As this example suggests, to avoid thermal errors in reconstructed data products, calibration data must be taken frequently or precise thermal stability of the system must be maintained actively. Both of these solutions complicate field deployment significantly. An alternative self-calibration technique has been developed in attempts to circumvent these thermal errors [7]. However, this calibration method does not provide for direct measurement of all CSP retarder phase values, leading to uncertainty in the calibration. Instead, if a thermally insensitive (TI) retarder can be produced, the reference beam calibration technique can be used without the need for frequent recalibration.

A TI retarder can be produced by taking advantage of the three distinct indices of refraction in a biaxial crystal. Previous work by others produced a biaxial thermally insensitive (BTI) crystal for an unrelated application using potassium titanyl phosphate (KTP) [9]. By modifying the BTI design presented in [9] to produce a high order TI retarder for channeled spectropolarimetry, an athermal channeled spectropolarimeter (ACSP) can be produced. To simulate the polarimetric reconstruction errors that can

be anticipated with a KTP-based ACSP setup, the simulation scenario presented in Fig. 2 (a) was repeated with BTI KTP retarders instead of quartz. Fig. 2 (b) depicts the reconstructed Stokes parameters for a 5°C temperature change using the ACSP system. Comparing to the results in Fig. 2 (a), the reconstructed Stokes parameters demonstrate a significantly enhanced correspondence to the input polarization state.

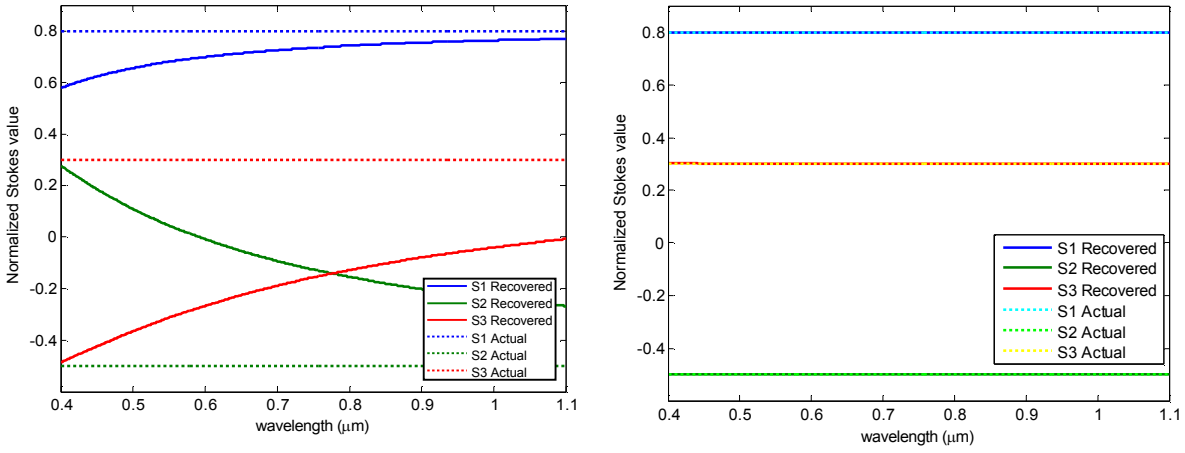

Fig. 2. Example of thermally induced reconstruction errors in Stokes parameters S_1, S_2, and S_3, across the VISNIR produced in (a) a conventional CSP system using quartz, and (b) a KTP ACSP system. A 5 °C change in temperature between calibration and data acquisition was used.

Alternatively, the use of multiple crystal materials has also been proposed and demonstrated as an approach to producing such a TI retarder [8]. A comparison of the BTI thermal stabilization results to the multi-material approach will be discussed in section 4.

2. LABORATORY PROTOTYPE

Proof of concept experiments in the visible spectral region were performed to provide experimental verification of the ACSP concept [10]. A diagram of the measurement methodology is depicted in Fig. 3 (a). A quartz tungsten halogen (QTH) lamp serves a collimated white light source. A generating polarizer (*G*) creates a known and stable input polarization state. The BTI retarder (*R*) is made of KTP and has a nominal thickness of l = 4.75 mm, and is cut to the athermal prescription described in [9], as depicted in Fig. 3 (b). The BTI retarder is aligned with its *y*-axis (as labeled in Fig. 3 (b)) at 45° relative to the horizontal and is mechanically mounted to a hotplate. This is followed by an analyzing polarizer (*A*) to unify the polarization state.

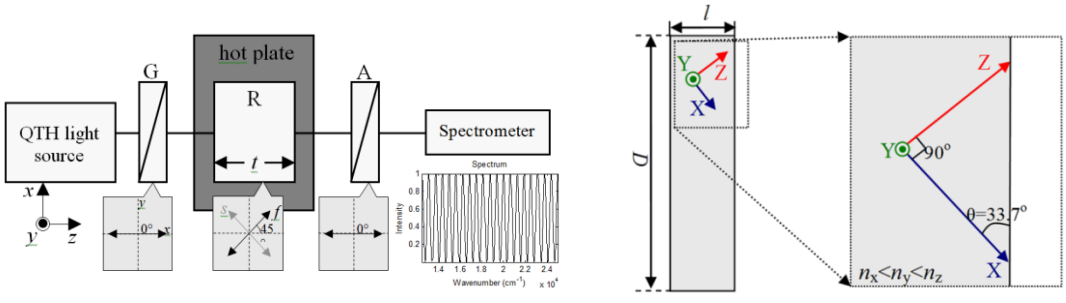

Fig. 3. ACSP design and testing. (a) Experimental setup for proof of concept testing of a partial ACSP using the BTI-cut KTP retarder. (b) The BTI retarder is produced using the TI-angle identified by Ebbers [9].

For the spectral measurement, the output of the analyzer is focused into a fiber that is connected to an Ocean Optics HR2000 UV-Vis spectrometer operating over a spectral range of λ = 200-1100 nm with a pixel resolution of 0.44 nm. Overall, based on the optical component's spectral passbands, the system is capable of spectropolarimetric measurements over wavelengths spanning 500 to 750 nm.

When using a single high order BTI retarder, the system operates as a partial channeled spectropolarimeter. The configuration depicted in Fig. 3 (a) is capable of measuring S_1 and S_3, with intensity I given by Eq. 1 with $\phi_1 = 0$, or

$$I(\sigma) = \frac{1}{2}\left[S_0(\sigma) + S_1(\sigma)\cos\left(\phi(\sigma)\right) - S_3(\sigma)\sin\left(\phi(\sigma)\right)\right], \tag{3}$$

where $\phi(\sigma) = 2\pi\sigma(n_y - n_{xz})l$ is the phase difference introduced by the KTP retarder. The effective index n_{xz} is the index of refraction in the xz-plane (perpendicular to n_y), given by

$$n_{xz} = \frac{n_x n_z}{\sqrt{n_x^2 \sin^2(\theta) + n_z^2 \cos^2(\theta)}}. \tag{4}$$

In Eq. 4, θ is defined relative to the face of the retarder, as indicated in Fig. 3 (b). For TI performance, $\theta = 33.7^o$ (+/- 0.5^o) was used when specifying the crystal axes orientation for retarder fabrication. Using λ=700 nm, $n_{xz}(\lambda)$~1.785, $n_y(\lambda)$~1.764, the OPD introduced by the BTI retarder is approximately 97 μm.

3. EXPERIMENTAL RESULTS

The temperature of the crystal was varied via thermal conduction using the hotplate. Temperature monitoring was accomplished using two thermocouples placed along the perimeter (non-imaging side) of the crystal approximately 180° apart. Fig. 4 (a) provides simulated spectra for the ACSP setup, using an estimate of the QTH source spectrum, for three different crystal temperatures ranging from ambient room temperature to 21° C above ambient. Fig. 4 (b) depicts the experimentally measured modulated spectra acquired using the ACSP prototype. Note that in both cases, the frequencies of the modulations are invariant as a function of temperature and therefore exhibit the desired TI properties.

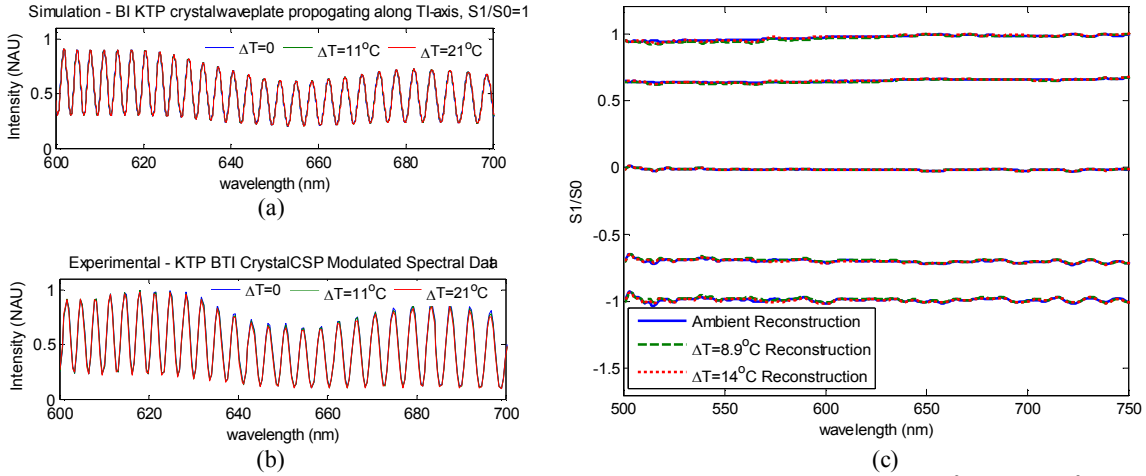

Fig. 4. Simulated (a) and experimental (b) ACSP modulated spectral data for ambient, +11 °C and +21 °C above ambient. The consistency in the carrier frequency is indicative of the thermal stability of the retarder. Example reconstructions from the ACSP prototype are depicted in (c).

To quantify the thermally-induced errors in reconstructed spectropolarimetric data products, the generating polarizer G was used to produce different linear input polarization states ranging from horizontal (0^o, $S_1/S_0 = 1$) to vertical (90^o, $S_1/S_0 = -1$) in 22.5^o increments. Note that while the ACSP prototype is capable of measuring S_3, G can only produce linear polarization states and a measurement of S_1 is sufficient for demonstrating the ACSP concept. Each state was measured with the prototype system at the ambient room temperature of 21.4 ^{o}C. Additionally, a reference polarization measurement at 157^o (S_1/S_0=0.707) was also obtained at the ambient room temperature. Next, the retarder was heated to temperatures of 30.3 ^{o}C and 35.6 ^{o}C and two additional reference measurements were obtained. Fig. 4 (c) depicts the reconstructed S_1 Stokes parameter that was produced using the three different reference measurements over the λ = 500-750 nm spectral range. Overall, the reconstructed values agree to within 1.0% RMS, and these data indicate that the spectropolarimetric reconstructions produced from this ACSP system exhibit minimal changes when the system experiences a change in temperature less than or equal to 14^o C.

Finally, the experiment described above was repeated for a series of temperatures ranging from 13.3 ^{o}C to 25.7 ^{o}C above ambient. The RMS error in the reconstructed S_1 values when comparing the ambient and increased temperature reference measurements over λ = 500-750 nm are provided in Table 1. These results provide an initial quantification of the anticipated error for a given change in temperature for this KTP-based ACSP system. For comparison, a simulated partial CSP using an equivalent quartz retarder yields a reconstruction error of 183% RMS for a temperature increase from 21.4°C to 49.8°C.

Table 1. RMS error in ACSP reconstructions using ambient versus high temperature reference data.

	ΔT=13.3^{o}C	ΔT=19.9^{o}C	ΔT=25.7^{o}C
S1/S0=1.0	1.9%	3.8%	5.2%
S1/S0=0.7	1.4%	2.9%	3.8%
S1/S0=0.0	0.2%	0.3%	0.4%
S1/S0=-0.7	1.8%	3.5%	4.6%
S1/S0=-1.0	2.6%	5.2%	6.7%

4. COMPARISON TO A MULTI-MATERIAL APPROACH

As previously mentioned, a multi-material approach for thermally stabilizing the retarders used for CSP has been suggested and demonstrated by Snik et al. [8] using MgF_2 and AlO_3 (sapphire). Using an optimized thickness ratio for each material (2.3:1 was used for MgF_2:AlO_3), the combination of the thermo-optic constants of each material results in a composite phase delay that is nearly independent of temperature at a given wavelength. The approach was experimentally demonstrated using 1.10 mm of AlO_3 and 2.53 mm of MgF2 (together introducing approximately 21 μm of OPD) and the maximum residual phase error was found to be 1.5 x 10^{-2} rad/^{o}C over 550-750 nm. This experimentally measured value is in reasonable correspondence to the maximum phase error calculated using published values for the thermo-optic constants of these materials [11], found to be 7.2 x 10^{-3} rad/^{o}C. As cited in [8], some of this discrepancy is likely caused by uncertainty in the thermo-optic constants for these materials over the entire passband of interest.

To provide a comparison between the multi-material athermal retarder and the BTI retarder presented in the previous sections, the residual phase change (RPC) introduced by the multi-material design is assumed to be linear with retarder thickness and temperature change. Based on the experimentally measured RPC cited in [8], a MgF2-AlO3 retarder that introduces the same amount of OPD as the BTI retarder (97 μm) can be expected to introduce a maximum RPC of 1.46 rad for a temperature change of 21 ^{o}C. Conversely, using the experimental data acquired in section 3, Fig. 5 depicts the RPC for the KTP BTI approach for a temperature change of 21 ^{o}C. The maximum RPC for the KTP BTI retarder over 550-750 nm is 0.270 rad, which is over a factor of 5 improvement in thermal stability versus the multi-

material approach. For comparison, the RPCs for the BTI and multi-material approaches calculated using the tabulated thermo-optic coefficient values of KTP [12], MgF2, and AlO3 [11] are also depicted in Fig. 5. There is appreciable discrepancy between the experimentally measured and anticipated RPC values for KTP, but both curves demonstrate significantly smaller RPC over the spectral passband versus the multi-material approach. While additional materials can be added to the multi-material approach to introduce more degrees of freedom and further reduce the residual error, this process increases design complexity, cost, and size, particularly for the high order retarders needed for CSP.

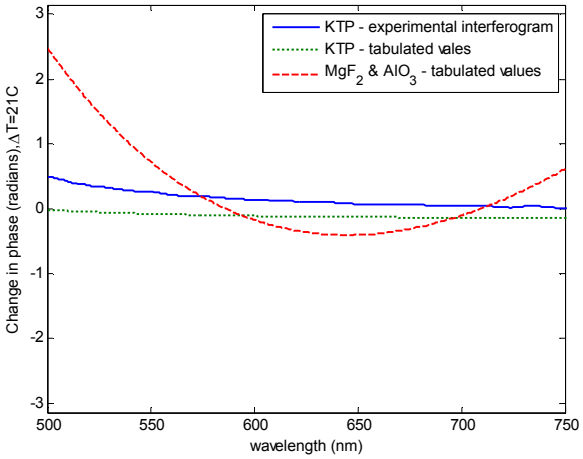

Fig. 5. Comparison of RPC for the two TI retarder approaches. The experimentally measured KTP BTI RPC and the anticipated RPC, based on tabulated thermo-optic coefficients, for the KTP BTI approach are depicted along with the anticipated RPC for the multi-material approach.

This comparison of these two approaches is based on the performance of initial TI retarder designs in the visible spectral regime. In general, the RPC produced by either approach will vary depending on the materials selected. Furthermore, there are other considerations that may inform the selection of one thermal stabilization approach over the other. For example, certain systems may not be able to accommodate multiple retarder materials due to size and weight concerns, or the material needed for one approach may be unavailable or difficult to obtain. The obvious design limitation for the BTI approach is the limited range of angles over which the biaxial crystal provides sufficient thermal stability, which must be considered when applying this approach in an imaging system. This is explored in the next section.

5. SNAPSHOT IMAGING SPECTROPOLARIMETER DESIGN

Based on the results from the ACSP proof of concept experiments in the visible, a design concept for a short wavelength infrared (SWIR) snapshot imaging spectropolarimeter system is currently under development. The system is referred to as the snapshot compact athermal multispectral polarimetric imager (SCAMPI) and combines the athermal CSP concept with a snapshot image slicing spectrometer (ISS) to provide a complete linear spectropolarimetric measurement in a single integration time.

The ISS concept was originally developed for astronomical applications [13-16] and more recently applied to high resolution microscopy in the visible [17-19]. For SCAMPI, the ISS technique has been implemented to produce a remote sensing system operating over the passband of InGaAs detectors in the SWIR (λ = 0.9 - 1.7 μm).

A two retarder design could be used to provide a complete polarization measurement for SCAMPI. However, for remote sensing applications, measurement of S_3 is often unnecessary as S_3 is infrequently observed in passive remote sensing [20]. Instead, measurement of S_1 and S_2 to quantify linear polarization signatures is preferable. Furthermore, measurement of S_1 and S_2 in a single CSP channel maximizes the

spectral resolution of each Stokes parameter measurement and improves the SNR of the S_2 measurement by a factor of 2 versus a conventional two element CSP approach. Thus, SCAMPI implements a partial CSP design using a single TI retarder element, similar to the ACSP prototype discussed in sections 2 and 3. To allow for measurement of S_1 and S_2 from a single channel, instead of S_1 and S_3, an achromatic quarter wave retarder (such as a TIR prism) is incorporated before the TI element. Assuming the analyzer is an ideal polarization element with an infinite extinction ratio, the spectral intensity for each (x_0, y_0) spatial point measured is given by

$$I(\sigma)=\frac{1}{2}\left[S_0(\sigma)+S_1(\sigma)\cos\left(\phi(\sigma)\right)+S_2(\sigma)\sin\left(\phi(\sigma)\right)\right]. \tag{5}$$

A Zemax layout of the SCAMPI optical design is depicted in Fig. 6. The polarization analyzing elements are incorporated before the imaging optics and the ISS elements. After passing through the ACSP optics, foreoptics are used to image the scene onto a reflective image slicer, which provides an image mapping capability that will be discussed shortly. Upon reflection, the light is relayed to a dispersive prism. Finally, a lenslet array is used to image the dispersed image slices onto an FPA. The SCAMPI system operates at f/3.6, with a 23.6 mm effective focal length and a +/-2.5^o full field of view (FFOV).

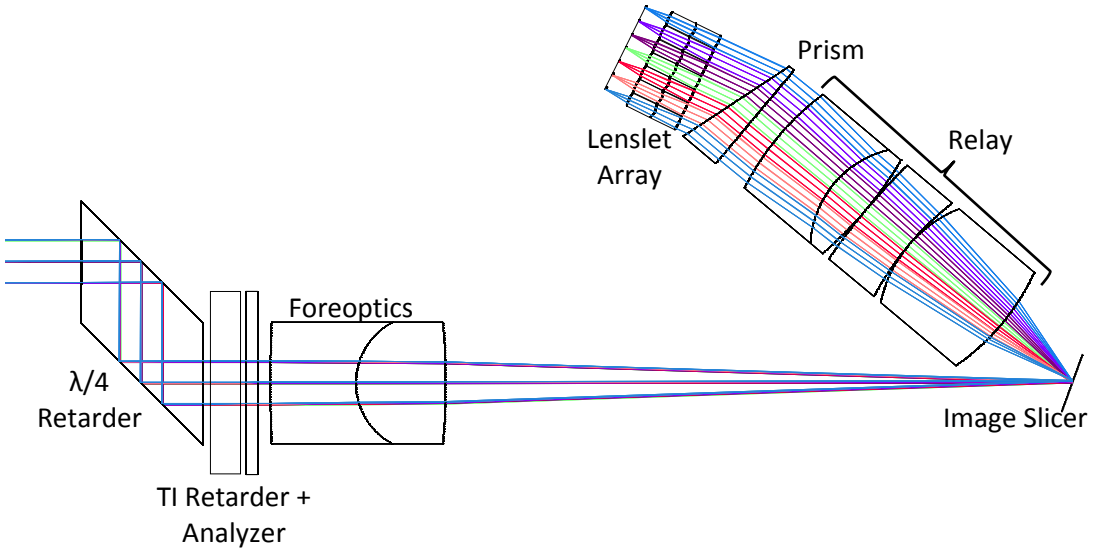

Fig. 6. Zemax layout of the SCAMPI prototype. The system is designed to operate in the SWIR. Combining an ACSP with an image slicing spectrometer, the system operates as a snapshot imaging spectropolarimeter.

The image slicer component is fundamental to the snapshot operation of SCAMPI. By separating an image into a number of one dimensional spatial slices that are then dispersed by the prism element, the image slicer functions as a number simultaneously operating pushbroom spectrometers that together capture a full spectral data cube. Fig. 7 depicts the dispersed image slice concept. For SCAMPI, the slicer is designed to couple with a 1024 by 1280 pixel InGaAs FPA with a 15 μm pixel pitch.

In principle, an ISS has the flexibility to be designed for any combination of spatial and spectral resolutions that results in a total sampling that equals the total number of pixels on the FPA. However in practice there are some limiting factors, such as image slicer feature size and the FOV for each sub-image, which bound the achievable spatial and spectral resolutions to a much smaller design space. In the case of SCAMPI, the desired +/- 2.5 degree FFOV results in a design that produces a spatial sampling of 146 by 128 pixels over the FFOV and 70 spectral samples over λ = 0.9 – 1.7 μm.

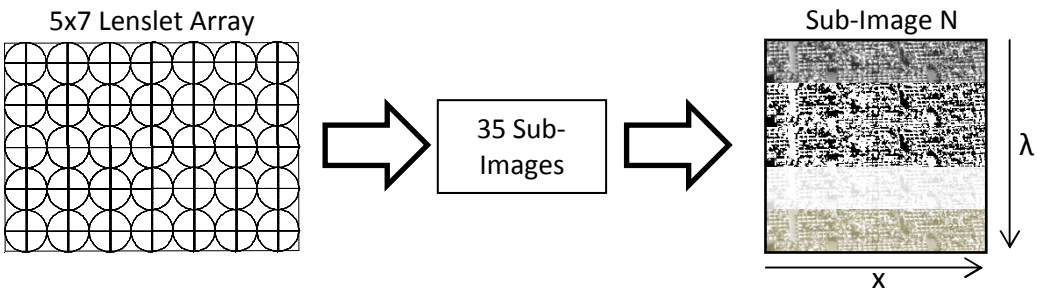

Fig. 7. The SCAMPI image slicer spectrometer incorporates a 5 by 7 lenslet array that produces 35 sub-images, each containing the dispersed and CSP-modulated spectra for a one dimensional slice of the composite image.

The TI retarder for SCAMPI can be produced using either the BTI or the multi-material approach. The performance of a BTI retarder is considered first. Due to its demonstrated athermal properties and high transmission in the SWIR, KTP was selected for the BTI retarder design. While the TI angle, θ_{TI} for KTP has been experimentally verified to be 33.7° relative to the *z*-axis at $\lambda = 0.633$ μm, to our knowledge, no experimental study has been conducted to identify θ_{TI} for KTP in the SWIR. Tabulated values for the thermo-optic properties of KTP can be used to calculated θ_{TI} using [9]

$$\theta_{TI} = \arccos\left(\frac{\frac{dn_z}{dT} - \frac{dn_y}{dT}}{\frac{dn_z}{dT} - \frac{dn_x}{dT}}\right)^{1/2} . \quad (6)$$

From Eq. 6, $\theta_{TI} = 32.6°$ is found for $\lambda = 1.3$ μm. While TI angle calculations based on tabulated thermo-optic properties are too inaccurate to provide for an estimate of the TI angle without experimental validation, this value for θ_{TI} is used for this initial design, keeping in mind an experimental validation should be performed before the BTI design for SCAMPI is finalized. Based on the spectral resolution of SCAMPI, a TI retarder element that introduces ~28 μm of OPD ensures sufficient fringe sampling across the spectral passband. For KTP and using $\theta_{TI} = 32.6°$, a 1.65 mm thick retarder introduces ~27.7 μm of OPD was modeled.

The thermal stability of the ACSP design was simulated over the +/- 2.5° FFOV of the SCAMPI sensor. For this initial design, the thermal stability was investigated for field angles in the the *xz*-plane (see Fig. 3 (b)) of the crystal exclusively. Thus light incident on the crystal in these simulations experiences indices n_y and $n_{xz}(\theta)$, where $n_{xz}(\theta)$ is defined by Eq. 4. Due to the relatively small FFOV of the SCAMPI sensor, the index variation in the *xz*-plane is anticipated to be the dominant variable affecting the thermal stability of the system.

Fig. 8 (a) depicts the simulated RPC for the KTP BTI design for temperature changes up to +/-25 °C. The maximum RPC under these conditions is $\Delta\phi = 5.8 \times 10^{-2}$ rad at $\lambda = 1.3$ μm, or 2.3×10^{-3} rad/°C. The simulated maximum RPC over the operational passband of the sensor is depicted in Fig. 8 (b) for the nominal value of θ_{TI}. Assuming that the fabrication tolerance on the axes orientations for the BTI element can be specified at +/-0.5° (as was the case for the visible prototype), Fig. 8 (b) also depicts maximum RPC for deviations of θ_{TI} from the nominal value of +/-0.5°. The overall maximum RPC for this BTI design is anticipated to be less than 5.2×10^{-3} rad/°C.

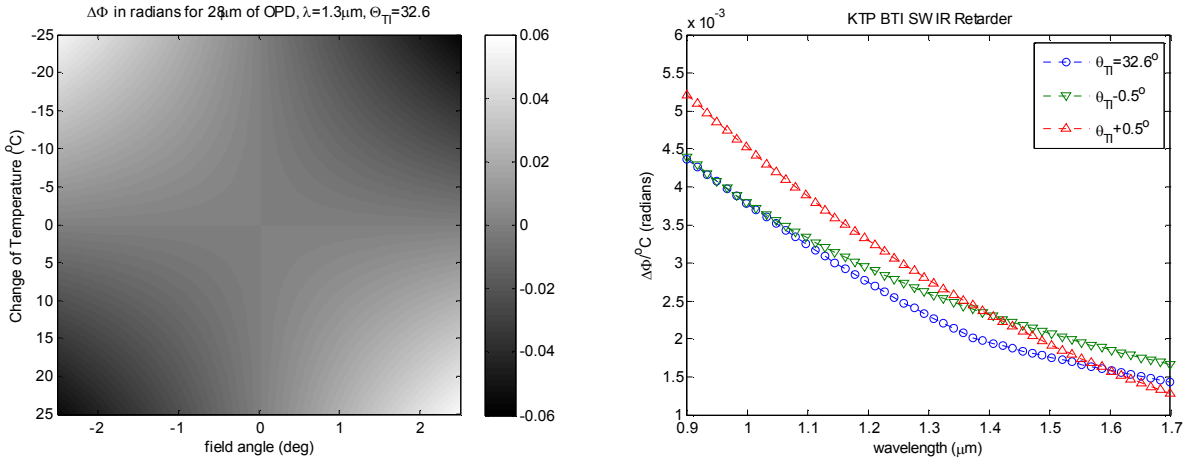

(a) (b)

Fig. 8. Residual phase change (RPC) for the KTP BTI retarder design for SCAMPI. The RPC as a function of field angle and change of temperature is depicted in (a) for λ=1.3 μm. The maximum RPC as a function of wavelength over the sensor passband is depicted in (b).

A multi-material approach using MgF_2 and AlO_3 was also investigated for producing a TI retarder for SCAMPI. The thickness ratio of the original visible spectrum design was modified to minimize the total phase error over the SCAMPI passband. For a 1:5.5 thickness ratio, a 0.50 mm thick AlO_3 retarder combined with a 2.75 mm MgF2 retarder together introduce 27.9 μm of OPD. The maximum RCP over $\lambda = 0.9 - 1.7$ μm for this multi-material design is $\Delta\phi = 0.21$ rad/°C, which is two orders of magnitude larger than the anticipated residual phase error for the KTP BTI approach. Thus, the thermal stabilizing properties of these materials that have been demonstrated in the visible do not extend to the SWIR. Although other materials may provide improved thermal stabilization in the SWIR over MgF_2 and AlO_3, for the initial design of SCAMPI, the BTI approach was pursued for producing the thermally stable spectropolarimetric measurement.

Using the reconstruction equations for the reference beam calibration technique [7], the variations in the normalized Stokes parameter reconstructions caused by thermal variability are given by

$$\hat{S}_{1,out} = \hat{S}_{1in}\cos(\Delta\phi) - \hat{S}_{2in}\sin(\Delta\phi), \text{ and} \tag{7}$$

$$\hat{S}_{2,out} = \hat{S}_{1,in}\sin(\Delta\phi) + \hat{S}_{2,in}\cos(\Delta\phi). \tag{8}$$

In Eqs. 7 and 8, the '^' denotes normalized Stokes parameters, the subscript '*out*' indicates the reconstructed values, the subscript '*in*' indicates the true Stokes parameter values, and $\Delta\phi$ denotes the RPC of the BTI retarder. Because S_1 and S_2 are measured in a single channel, the reconstruction errors for these Stokes parameters are coupled. Thus the maximum reconstruction error in S_1 for a change in retarder phase of $\Delta\phi$ is dependent on the amplitude of S_1 as well as the amplitude of S_2. For example, maximum reconstruction error in S_1 at λ= 1.3 μm for the SCAMPI design occurs for S_1=0.0303S_0 and S_2=0.9995S_0, while the minimum error in S_1 occurs for S_1=S_0 and S_2=0. The deviations in the reconstructed Stokes values ($|\hat{S}_{1,out} - \hat{S}_{1in}|$) are simulated in Fig. 9 for these two cases and are linear with temperature variation. For the case simulated in Fig. 9 (a), the deviation in the reconstructed normalized S_1 value at the 2.5° field angle is 2.65 x 10^{-3}/°C and is 8.77 x 10^{-5}/°C for the case simulated in Fig. 9 (b). While in some circumstances the edges of the FFOV are subject to large deviations in Stokes parameter reconstructions for large temperature changes, the majority of the SCAMPI field of view enjoys low reconstruction errors for substantial temperature changes.

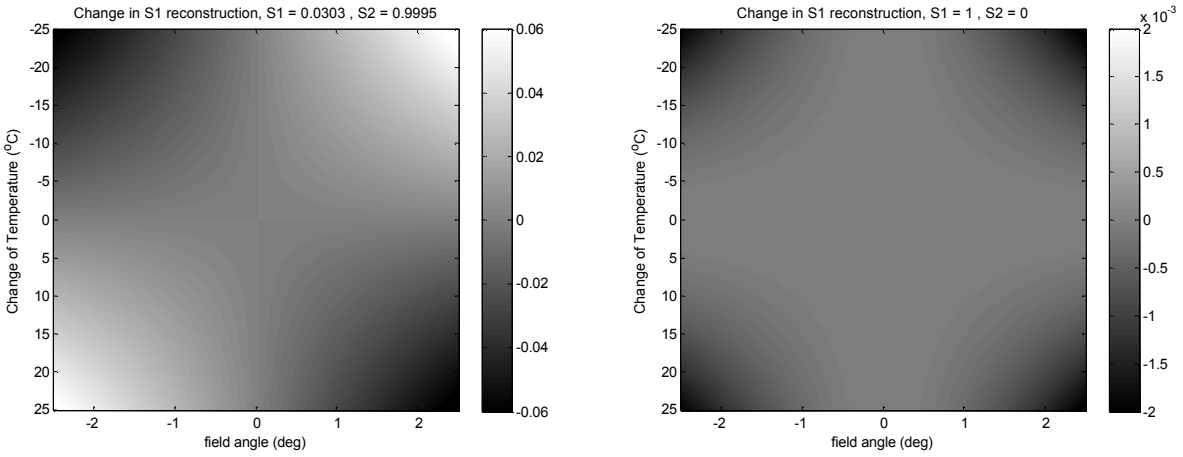

(a) (b)

Fig. 9. Deviations in the reconstructed Stokes parameters for the Stokes parameter values producing (a) the maximum reconstruction error and (b) the minimum reconstruction error.

Using the spectral resolution of the SCAMPI system, Fig. 10 (a) and (b) simulate the fringe profile for the on-axis and (2.5°, 0°) field points, respectively. The fringe profiles are depicted for temperature changes up to 25 °C and demonstrate the anticipated thermal stability of the retarder's carrier frequency over this temperature range.

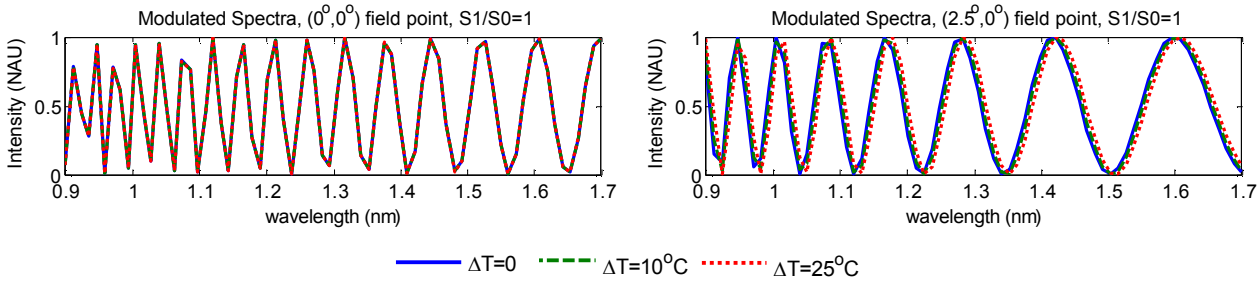

(a) (b)

Fig. 10. Fringe profiles for (a) the on-axis field point and (b) the (2.5 °, 0°) field point for the SCAMPI design using a KTP BTI retarder.

6. CONCLUSIONS

This paper presents a technique that provides enhanced thermal stability for CSP retarders versus the previous state of the art. While the design work presented in this paper is focused on athermalizing a channeled spectropolarimeter system specifically for remote sensing applications, nearly every application of channeled spectropolarimetry can benefit from a reduced need to recalibrate or update calibration data. The BTI technique utilizes readily available and inexpensive KTP to provide an athermalized CSP solution through the SWIR. However, it is worth nothing that there are other materials, such as RTA and LiISe [21] that possess the biaxial orthorhombic crystal properties that could potentially expand the implementation of this ACSP technique to the MWIR and LWIR.

Based on the results of initial proof of concept studies, a system that can provide snapshot imaging spectropolarimetric measurements in the SWIR is under development. The snapshot compact athermal multispectral polarimetric imager (SCAMPI) uses the thermally stable BTI retarder concept combined with an image slicing spectrometer to produce a snapshot spectropolarimetric measurement over a 5 degree FFOV and λ = 0.9-1.7 μm using 146 by 128 spatial samples and 70 spectral samples.

Future work will be focused on further development of the SCAMPI prototype and demonstration of the utility of this snapshot measurement capability for remote sensing.

7. ACKNOWLEDGEMENTS

This work was funded in part by NNSA/NA221, Victoria Franques, Program Manager. Sandia National Laboratories is a multi-program laboratory managed and operated by Sandia Corporation, a wholly owned subsidiary of Lockheed Martin Corporation, for the U.S. Department of Energy's National Nuclear Security Administration under contract DE-AC04-94AL85000. SAND # 2013-XXX.

REFERENCES

1. K.H. Nordsieck, "A simple polarimetric system for the Lick Observatory Image-Tube Scanner," Pub. Astron. Soc. Pac. 86(511) 324 – 329 (1974).
2. K. Oka, and T. Kato, "Spectroscopic polarimetry with a channeled spectrum," Opt. Lett. 24, 1475-1477 (1999).
3. D. Sabatke, A. Locke, E.L. Dereniak, M. Descour, and J. Garcia. "Snapshot imaging spectropolarimeter," Opt. Eng. 41(5) 1048-1054 (2002).
4. S.H. Jones, F.J. Iannarilli, and P.L. Kebabian, "Realization of quantitative-grade fieldable snapshot imaging spectropolarimeter," Opt. Exp. 12(26) 6559 – 6573 (2004).
5. M. W. Kudenov, N. A. Hagen, E. L. Dereniak, and G. R.Gerhart, "Fourier transform channeled spectropolarimetry in the MWIR," Opt. Express 15, 12792–12805 (2007).
6. J. Craven-Jones, M.W. Kudenov, M.G. Stapelbroek, and E.L. Dereniak, "Infrared hyperspectral imaging polarimeter using birefringent prisms," *Appl. Opt.*, 50(8) 1170-1185 (2011).
7. A. Taniguchi, K. Oka, H. Okabe, and M. Hayakawa, "Stabilization of a channeled spectropolarimeter by self-calibration," Opt. Lett. 31, 3279-3281 (2006).
8. F. Snik, T. Karalidi, and C.U. Keller, "Spectral modulation for full linear polarimetry," Appl. Opt., 48(7) 1337-1346 (2009).
9. C. Ebbers, "Thermally insensitive, single-crystal, biaxial electro-optic modulators," J. Opt. Soc. Am. B 12(6) 1012-1020 (1995).
10. J. Craven-Jones, B.M. Way, M.K. Kudenov, and J.A. Mercier, "Athermalized channeled spectropolarimetry using a biaxial potassium titany phosphate crystal," Opt. Lett 38(10) 1657-1659 (2013).
11. G. Ghosh, *Handbook of Thermo-Optic Coefficients of Optical Materials with Applications*, Academic Press (1988).
12. W. Wiechmann, S. Kubota, T. Fukui, and H. Masuda, "Refractive-index temperature derivatives of potassium titanyl phosphate," Opt. Lett 18(15) 1208-1210 (1993).
13. L. Weitzel, A. Krabbe, H. Kroker, N. Thatte, L. E. Tacconi-Garman, M. Cameron, and R. Genzel, L. E. Tacconi Garman, M. Cameron and R. Genzel, "3D: The next generation near-infrared imaging spectrometer," Astron. Astrophys. Suppl. Ser. 119(3), 531–546 (1996).
14. S. Vivès, and E. Prieto, "Original image slicer designed for integral field spectroscopy with the near-infraredspectrograph for the James Webb Space Telescope," Opt. Eng. 45(9), 093001 (2006).
15. F. Henault, R. Bacon, R. Content, B. Lantz, F. Laurent, J. Lemonnier, and S. Morris, "Slicing the universe at affordable cost: the quest for the MUSE image slicer," Proc. SPIE 5249, 134–145 (2004).
16. J. A. Smith, "Basic principles of integral field spectroscopy," N. Astron. Rev. 50(4-5), 244–251 (2006).
17. L. Gao, R.T. Kester, and T.S. Tkaczyk, "Compact image slicing spectrometer (ISS) for hyperspectral fluorescence microscopy," Opt. Exp. 17(5) 12293-12308 (2009).
18. L. Gao, R.T. Kester, N. Hagen and T.S. Tkaczyk, "Snapshot Image Mapping Spectrometer (IMS) with high sampling density for hyperspectral microscopy," Opt. Exp. 18(14) 14330-14344 (2010).
19. N Bedard, N. Hagen, L. Gao, and T.S. Tkaczyk, "Image mapping spectrometry: calibration and characterization," Opt. Eng. 51(11) 111711 (2012).
20. J.S. Tyo, D.L. Goldstein, D.B. Chenault, and J.A. Shaw, "Review of passive imaging polarimetry for remote sensing applications," Appl. Opt. 45(22) 5453 – 5469 (2006).

21. B.M. Way, “Performance enhancement of a channeled spectropolarimeter by athermalization,” MS Thesis, University of New Mexico, pp.21-24, (2013).